

# Three-body gravitino decays in the MSSM

Helmut Eberl<sup>1</sup> and Vassilis C. Spanos<sup>2</sup>

<sup>1</sup>*Institut für Hochenergiephysik der Österreichischen Akademie der Wissenschaften,  
A-1050 Vienna, Austria*

<sup>2</sup>*Institute of Nuclear and Particle Physics, NCSR “Demokritos”, GR-15310 Athens,  
Greece*

## Abstract

We present results from a new calculation of two- and three-body decays of the gravitino including all possible Feynman graphs. The work is done in the  $R$ -parity conserving Minimal Supersymmetric Standard Model, assuming that the gravitino is unstable. We calculate the full width for the three-body decay process  $\tilde{G} \rightarrow \tilde{\chi}_1^0 X Y$ , where  $\tilde{\chi}_1^0$  is the lightest neutralino that plays the role of the lightest supersymmetric particle, and  $X, Y$  are standard model particles. For calculating the squared amplitudes we use the packages `FeynArts` and `FormCalc`, with appropriate extensions to accommodate the gravitino with spin  $3/2$ . Our code treats automatically the intermediate exchanged particles that are on their mass shell, using the narrow width approximation. This method considerably simplifies the complexity of the evaluation of the total gravitino width and stabilizes it numerically. At various points of the supersymmetric parameter space, we compare the full two-body and the three-body results with approximations used in the past. In addition, we discuss the relative sizes of the full two-body and the three-body gravitino decay widths. Our results are obtained using the package `GravitinoPack`, that will be publicly available soon, including various handy features.

# 1 Introduction

The gravitino, the supersymmetric partner of the graviton, is part of the particle spectrum of extensions of the Standard Model (SM) that incorporate the local version of supersymmetry, the supergravity. Depending on the mass hierarchy of these models, in the case of  $R$ -parity conservation, the gravitino can be either the stable lightest supersymmetric particle (LSP) that plays the role of the dark matter particle, or it is heavier than the LSP and thus unstable. In the latter case, it is important to calculate precisely the width of the gravitino decays to the lightest neutralino ( $\tilde{\chi}_1^0$ ), that naturally is the LSP in this case, and other SM particles. The precise value of the gravitino lifetime is probably the most important parameter that affects the primordial Big-Bang Nucleosynthesis (BBN) constraints, assuming that it decays during or after the BBN time. Indeed, the abundances of the light nuclei, like D,  $^4\text{He}$ ,  $^3\text{He}$  and  $^7\text{Li}$  produced during the BBN epoch, provide very stringent constraints on the decays of unstable massive particles during the early Universe [1–16].

The astrophysical measurements of the abundances of various light elements agree well with those predicted by the homogeneous BBN calculations. Thereby, it is assumed that the baryon-to-photon ratio  $\eta$  required for these calculations [17] agrees very well with that inferred [18] from observations of the power spectrum of fluctuations in the cosmic microwave background. On the other hand, the value of  $\eta$  that they provide is now quite precise, reducing the main uncertainty in the BBN calculation. The decays of massive unstable particles, like the gravitino, could have destroyed this concordance because the electromagnetic and/or hadronic showers they produced might have either destroyed or created the light nuclear species. In this calculation, probably the most important parameter is the lifetime of the unstable gravitino, because it dictates the cosmic time when these injections will occur [15].

In the previous studies the dominant two-body decays of the gravitino have been considered, that is the processes  $\tilde{G} \rightarrow \tilde{X} Y$ , where  $\tilde{X}$  is a sparticle, and  $Y$  a SM particle. These two-body decays dominate the total gravitino width, and in particular the channel  $\tilde{G} \rightarrow \tilde{\chi}_1^0 \gamma$ , which is kinematically open in the whole region of the neutralino LSP model,  $m_{\tilde{G}} > m_{\tilde{\chi}_1^0}$ . This channel is also important because it provides the bulk of the electromagnetic energy produced by the gravitino decays. On the other hand, the decay  $\tilde{G} \rightarrow \tilde{\chi}_1^0 Z$  is the dominant channel that produces hadronic products. Since, these decays are of “gravitational nature”, the gravitino width is proportional to  $M_P^{-2}$ , where  $M_P = 1/\sqrt{8\pi G_N}$  is the reduced Planck mass, and its lifetime is of the order of few sec-

onds or more. Afterwards, the produced sparticle  $\tilde{X}$  decays almost instantaneously in comparison to the gravitational decay, like  $\tilde{X} \rightarrow \tilde{\chi}_1^0 X$ , where  $X$  is a SM particle. So, assuming that the dominant two-body channel is kinematically possible,  $m_{\tilde{G}} > m_{\tilde{X}} + m_Y$ , the gravitino decays to the LSP  $\tilde{\chi}_1^0$  as

$$\tilde{G} \xrightarrow{grav} \tilde{X} Y \xrightarrow{EW} \tilde{\chi}_1^0 X Y, \quad (1)$$

where, as it is indicated, the first decay is of gravitational and the second one of electroweak nature. If the primary two-body gravitino decay channel is not open,  $m_{\tilde{G}} < m_{\tilde{X}} + m_Y$ , the three-body decay

$$\tilde{G} \xrightarrow{grav} \tilde{\chi}_1^0 X Y \quad (2)$$

is still possible, if  $m_{\tilde{G}} > m_{\tilde{\chi}_1^0} + m_X + m_Y$ , through off-shell particles exchange. Therefore, it is important to include the three-body channels, like  $\tilde{G} \rightarrow \tilde{\chi}_1^0 q \bar{q}$ , which inject hadrons in the cosmic plasma even below the threshold for the on-shell  $Z$ -boson production. This channel, together with the  $\tilde{G} \rightarrow \tilde{\chi}_1^0 W^+ W^-$ , usually have been taken into account in the previous studies. In particular, the channel  $\tilde{\chi}_1^0 W^+ W^-$  and its high energy behavior has been already studied in detail [15, 19], due to the tricky cancellation of the unitarity violating terms that are associated with the longitudinal components of the  $W$ -bosons.

The purpose of this paper is to present the complete calculation of the gravitino two-body decays, *as well as all the possible three-body* decay channels  $\tilde{G} \rightarrow \tilde{\chi}_1^0 X Y$ . This calculation provides us with a comprehensive picture of the gravitino decays above and *below* the kinematical thresholds of the two-body decays. For the computation of the gravitino decay amplitudes we use the **FeynArts** (FA) and **FormCalc** (FC) packages [20–22]. In order to be able to generate the amplitudes with FA we have extended its generic structures to interactions with spin-3/2 particles and built a model file with all possible gravitino interactions with the particles of the Minimal Supersymmetric Standard Model (MSSM). FC has been extended so that it automatically generates a FORTRAN code for the numerical calculation of the squared amplitudes. As there are many gamma matrices involved we have done this within FC by using the Weyl-van-der-Waerden formalism [23], as implemented into FC from [24].

Moreover, the code treats automatically the intermediate exchanged particles that are on their mass shell as unstable, using the narrow width approximation. By doing so, one avoids the double counting among the two- and three-body channels, but also the CPU-time consuming phase space integrations over the unstable exchanged particles in

the propagators. It also leads to a considerable simplification of the numerical evaluation of the total three-body gravitino width.

Our computer code will become publicly available soon as part of `GravitinoPack` [25]. This package supports the SUSY Les Houches Accord 2 format [26, 27] and works within the general flavour conserving MSSM with possibly complex input parameters. It incorporates handy FORTRAN and MATHEMATICA routines that evaluate two- and three-body gravitino decay widths. The code returns all partial decay widths (or branching ratios) for the individual decay channels.

As basis for our numerical study we use various benchmark points from supersymmetric models with different characteristics. In particular, we choose points based on the phenomenological MSSM (pMSSM), the Constrained MSSM (CMSSM) and the Non-Universal Higgs Model (NUHM). These points satisfy all the recent high energy constraints from the LHC experiments on the superpartner lower mass bounds, the Higgs boson mass  $\sim 126$  GeV, as well as the LHCb measurement on the rare decay  $B_s \rightarrow \mu^+ \mu^-$  that constrains supersymmetric models at the large  $\tan\beta$  regime. In addition, these points conform with the cosmological constraints on the amount of the neutralino relic density, measured by the Planck and the WMAP experiments.

Numerically we have found that the calculation of the full three-body decay amplitudes is important in the computation of the gravitino width for any gravitino mass, above and below the mass thresholds for the dominant two-body decay channels. Furthermore, we have compared the total gravitino decay width, up to the three-body level, with a previously used approximation. We have found that the full result can differ from the approximation by more than a factor of 2, especially for  $m_{\tilde{G}} \gtrsim 2$  TeV. This affects considerably the gravitino lifetime, which is an important parameter in constraining models with unstable gravitinos, using the BBN predictions. Interestingly enough, we have found that both goldstino ( $\pm\frac{1}{2}$ ) and the pure gravitino ( $\pm\frac{3}{2}$ ) spin states contribute comparably, even for large gravitino masses, up to 6 TeV or larger.

The paper is organized as: In section 2 the details of our calculation are explained. In particular, we analyse the gravitino interactions in the MSSM and we demonstrate, using specific examples, our implementation in the FA/FC code. Moreover, the calculation of the gravitino two- and three-body decay width is discussed. In section 3 we present the numerical results, using as basis various benchmark points from different supersymmetric models. Finally in section 4, we summarize our findings and give a perspective of our future work in this direction.

## 2 The calculation

### 2.1 Gravitino interactions within the MSSM

Our starting point is the Lagrangian that describes the gravitino interactions in the MSSM [28],

$$\begin{aligned} \mathcal{L}_{\tilde{G}, \text{int}}^{(\alpha)} = & -\frac{i}{\sqrt{2}M_{\text{P}}} \left[ \mathcal{D}_{\mu}^{(\alpha)} \phi^{*i} \overline{\tilde{G}}_{\nu} \gamma^{\mu} \gamma^{\nu} \chi_L^i - \mathcal{D}_{\mu}^{(\alpha)} \phi^i \overline{\chi}_L^i \gamma^{\nu} \gamma^{\mu} \tilde{G}_{\nu} \right] \\ & - \frac{i}{8M_{\text{P}}} \overline{\tilde{G}}_{\mu} [\gamma^{\nu}, \gamma^{\rho}] \gamma^{\mu} \lambda^{(\alpha)a} F_{\nu\rho}^{(\alpha)a} , \end{aligned} \quad (3)$$

with the covariant derivative given by

$$\mathcal{D}_{\mu}^{(\alpha)} \phi^i = \partial_{\mu} \phi^i + i g_{\alpha} A_{\mu}^{(\alpha)a} T_{a,ij}^{(\alpha)} \phi^j , \quad (4)$$

and the field strength tensor  $F_{\mu\nu}^{(\alpha)a}$  reads

$$F_{\mu\nu}^{(\alpha)a} = \partial_{\mu} A_{\nu}^{(\alpha)a} - \partial_{\nu} A_{\mu}^{(\alpha)a} - g_{\alpha} f^{(\alpha)abc} A_{\mu}^{(\alpha)b} A_{\nu}^{(\alpha)c} . \quad (5)$$

The index  $\alpha$  corresponds to the three groups  $U(1)_Y$ ,  $SU(2)_L$ , and  $SU(3)_c$  with  $a$  up to 1, 3, 8, respectively, and  $i = 1, 2, 3$ .  $\phi^i$ ,  $\chi^j$ ,  $A^a$ , and  $\lambda^a$  are the scalar, spin 1/2, gauge and gaugino fields of the MSSM, respectively, as given in the Tables 1 and 2 in [28].

We write the four polarisation states of the gravitino field in the momentum space in terms of spin-1 and spin-1/2 components as

$$\begin{aligned} \psi_{\mu}(\mathbf{k}, \frac{3}{2}) &= u(\mathbf{k}, \frac{1}{2}) \epsilon_{\mu}(\mathbf{k}, 1) , \\ \psi_{\mu}(\mathbf{k}, \frac{1}{2}) &= \sqrt{\frac{1}{3}} u(\mathbf{k}, -\frac{1}{2}) \epsilon_{\mu}(\mathbf{k}, 1) + \sqrt{\frac{2}{3}} u(\mathbf{k}, \frac{1}{2}) \epsilon_{\mu}(\mathbf{k}, 0) \\ \psi_{\mu}(\mathbf{k}, -\frac{1}{2}) &= \sqrt{\frac{1}{3}} u(\mathbf{k}, \frac{1}{2}) \epsilon_{\mu}(\mathbf{k}, -1) + \sqrt{\frac{2}{3}} u(\mathbf{k}, -\frac{1}{2}) \epsilon_{\mu}(\mathbf{k}, 0) \\ \psi_{\mu}(\mathbf{k}, -\frac{3}{2}) &= u(\mathbf{k}, -\frac{1}{2}) \epsilon_{\mu}(\mathbf{k}, -1) , \end{aligned} \quad (6)$$

with  $\mathbf{k}$  being the spatial part of the four momentum  $k^{\mu} = (k^0, |\mathbf{k}|\mathbf{e})$ , and  $\mathbf{e}$  the unit vector in the flight direction of the gravitino.

From the field equation for the spin-3/2 particle, the so called Rarita-Schwinger equation [29], we get three equations in momentum space, which we have to fulfill by the right choice of the spin-1 and spin-1/2 field components [30],

$$\gamma^{\mu} \psi_{\mu}(\mathbf{k}, \lambda) = 0 , \quad (7)$$

$$k^{\mu} \psi_{\mu}(\mathbf{k}, \lambda) = 0 , \quad (8)$$

$$(\not{k} - m_{\tilde{G}}) \psi_{\mu}(\mathbf{k}, \lambda) = 0 , \quad (9)$$

where  $m_{\tilde{G}}$  is the mass of the gravitino. We have checked that our implementation of  $\psi_\mu$  into FC indeed fulfills these three equations.

All possible structures for the gravitino interactions with the MSSM particles in Eq. (3), are depicted in Figure 1. We have extended the FA generic Lorentz file with these structures. The 78 couplings given by the coefficient vectors  $C[. . .]$ , have been appended to the FA MSSM model file. Further technical details will be provided in [25].

As an illustrative example, we will exhibit how we obtain the  $\tilde{\chi}_i^0 \tilde{G} W^+ W^-$  interaction Lagrangian, and the corresponding structure “struc1” in Figure 1 used in our numerical calculation. For this, we will need the term in the second line of Eq. (3) and from Eq. (5) the part that is proportional to the  $SU(2)_L$  gauge coupling constant  $g$ . In particular, we get  $\lambda^{(2)a} = \tilde{W}^3$ ,  $f^{(2)abc} = \epsilon^{abc}$  with  $\epsilon^{123} = 1$ , and  $A_\mu^{(2)1,2} = W_\mu^{1,2}$ . The relevant Lagrangian can be written as

$$\mathcal{L} = \frac{ig}{8M_{\text{P}}} \tilde{G}_\mu [\gamma^\nu, \gamma^\rho] \gamma^\mu \tilde{W}^3 (W_\nu^1 W_\rho^2 - W_\nu^2 W_\rho^1). \quad (10)$$

We write the field  $\tilde{W}^3$  in terms of the physical neutralino field as,  $\tilde{W}^3 = Z_{k,2}^* P_L \tilde{\chi}_k^0 + Z_{k,2} P_R \tilde{\chi}_k^0$  and the  $W_\mu^{1,2}$  components in terms of the physical  $W$ -boson fields as,  $W_\mu^1 = (W_\mu^+ + W_\mu^-)/\sqrt{2}$ ,  $W_\mu^2 = i(W_\mu^+ - W_\mu^-)/\sqrt{2}$ . Thus, we get

$$\mathcal{L} \sim \frac{g}{4M_{\text{P}}} W_\nu^+ W_\rho^- \tilde{G}_\mu [\gamma^\nu, \gamma^\rho] \gamma^\mu (Z_{i,2}^* P_L + Z_{i,2} P_R) \tilde{\chi}_i^0. \quad (11)$$

Making use of the reality of the Lagrangian, from the hermitian conjugate part one gets

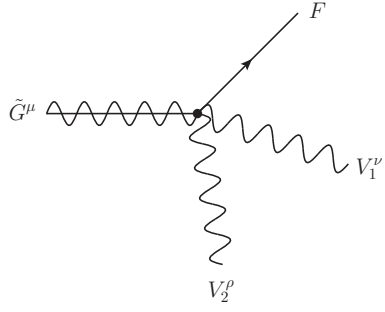
$$\mathcal{L} \sim \frac{g}{4M_{\text{P}}} W_\nu^+ W_\rho^- \tilde{\chi}_i^0 \gamma^\mu [\gamma^\nu, \gamma^\rho] (Z_{i,2} P_L + Z_{i,2}^* P_R) \tilde{G}_\mu. \quad (12)$$

From this formula we calculate the Feynman rule for the vertex in Figure 2. Finally, to obtain the FA structure “struc1”, given in Figure 1, we write the vertices for an incoming and outgoing gravitino by adding the terms from Eqs. (11) and (12) as

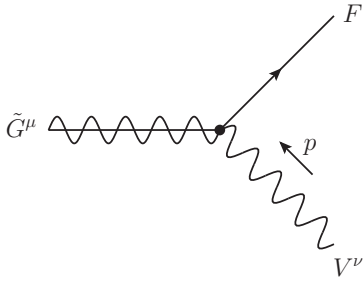
$$C[\tilde{\chi}_i^0, \tilde{G}_\mu, W_\nu^+, W_\rho^-]_{(1)} \gamma^\mu [\gamma^\nu, \gamma^\rho] P_L + C[\tilde{\chi}_i^0, \tilde{G}_\mu, W_\nu^+, W_\rho^-]_{(2)} \gamma^\mu [\gamma^\nu, \gamma^\rho] P_R + \\ C[\tilde{\chi}_i^0, \tilde{G}_\mu, W_\nu^+, W_\rho^-]_{(3)} [\gamma^\nu, \gamma^\rho] \gamma^\mu P_L + C[\tilde{\chi}_i^0, \tilde{G}_\mu, W_\nu^+, W_\rho^-]_{(4)} [\gamma^\nu, \gamma^\rho] \gamma^\mu P_R, \quad (13)$$

with the coupling vector

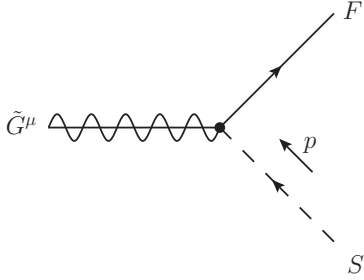
$$C[\tilde{\chi}_i^0, \tilde{G}_\mu, W_\nu^+, W_\rho^-]_{(1)} = i \frac{g}{4M_{\text{P}}} Z_{i,2}, \\ C[\tilde{\chi}_i^0, \tilde{G}_\mu, W_\nu^+, W_\rho^-]_{(2)} = i \frac{g}{4M_{\text{P}}} Z_{i,2}^*, \\ C[\tilde{\chi}_i^0, \tilde{G}_\mu, W_\nu^+, W_\rho^-]_{(3)} = i \frac{g}{4M_{\text{P}}} Z_{i,2}^*, \\ C[\tilde{\chi}_i^0, \tilde{G}_\mu, W_\nu^+, W_\rho^-]_{(4)} = i \frac{g}{4M_{\text{P}}} Z_{i,2}. \quad (14)$$



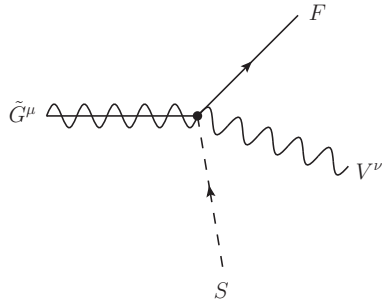
$$\text{struc1} : \begin{pmatrix} \gamma^\mu [\gamma^\nu, \gamma^\rho] P_L \\ \gamma^\mu [\gamma^\nu, \gamma^\rho] P_R \\ [\gamma^\nu, \gamma^\rho] \gamma^\mu P_L \\ [\gamma^\nu, \gamma^\rho] \gamma^\mu P_R \end{pmatrix} .C[F|\bar{F}, \tilde{G}^\mu, V_1^\nu, V_2^\rho]$$



$$\text{struc2} : \begin{pmatrix} \gamma^\mu \gamma^\nu P_L \\ \gamma^\mu \gamma^\nu P_R \\ \gamma^\mu [\gamma^\nu, \not{p}] P_L \\ \gamma^\mu [\gamma^\nu, \not{p}] P_R \\ \gamma^\nu \gamma^\mu P_L \\ \gamma^\nu \gamma^\mu P_R \\ [\gamma^\nu, \not{p}] \gamma^\mu P_L \\ [\gamma^\nu, \not{p}] \gamma^\mu P_R \end{pmatrix} .C[F|\bar{F}, \tilde{G}^\mu, V^\nu]$$



$$\text{struc3} : \begin{pmatrix} \gamma^\mu \not{p} P_L \\ \gamma^\mu \not{p} P_R \\ \not{p} \gamma^\mu P_L \\ \not{p} \gamma^\mu P_R \end{pmatrix} .C[F|\bar{F}, \tilde{G}^\mu, S]$$



$$\text{struc4} : \begin{pmatrix} \gamma^\mu \gamma^\nu P_L \\ \gamma^\mu \gamma^\nu P_R \\ \gamma^\nu \gamma^\mu P_L \\ \gamma^\nu \gamma^\mu P_R \end{pmatrix} .C[F|\bar{F}, \tilde{G}^\mu, V^\nu, S]$$

Figure 1: Possible structures of gravitino interactions with MSSM particles, detailed explanation is given in the text. As all momenta are defined incoming in FA,  $\partial_\mu \rightarrow -ip_\mu$ .

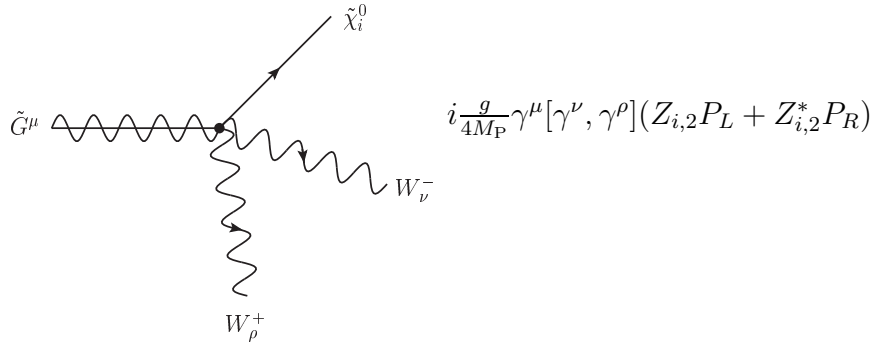


Figure 2: Feynman rule for  $\tilde{G} \rightarrow \tilde{\chi}_i^0 W^+ W^-$  four-particle interaction that corresponds to the Lagrangian in Eq. (12).

Note, that  $C[-, -, V_{1\nu}, V_{2\rho}]_{(i)} = -C[-, -, V_{2\nu}, V_{1\rho}]_{(i)}$ .

Similarly, we have calculated all the other coefficient vectors  $C[. . .]$  for the “struc1,2,3,4” shown in Figure 1, in order to get the full list of all possible gravitino interactions in the MSSM.

## 2.2 Two-body decays

The gravitino decays into a fermion  $F$ , and a scalar  $S$  or a vector particle  $V$  are

$$\begin{aligned}
 \tilde{G} &\rightarrow F S \\
 &\rightarrow f \tilde{f}_i^*, \tilde{\chi}_j^0 (h^0, H^0, A^0), \tilde{\chi}_k^+ H^-, \\
 \tilde{G} &\rightarrow F V \\
 &\rightarrow \tilde{g} g, \tilde{\chi}_j^0 (Z^0, \gamma), \tilde{\chi}_k^+ W^-,
 \end{aligned} \tag{15}$$

where  $f$  denotes a SM fermion, quarks  $(u, d, c, s, t, b)$  and leptons  $(e^-, \mu^-, \tau^-, \nu_e, \nu_\mu, \nu_\tau)$ . Its corresponding superpartners are the squarks  $\tilde{f}_i$ ,  $i = 1, 2$ . The four neutralino states are  $\tilde{\chi}_j^0$ ,  $j = 1, \dots, 4$  and the two charginos  $\tilde{\chi}_k^\pm$ ,  $k = 1, 2$ . With  $g$  we denote the gluon and with  $\tilde{g}$  its superpartner, the gluino. Furthermore, in the MSSM we have three neutral Higgs bosons (two  $CP$ -even:  $h^0$  and  $H^0$ , and one  $CP$ -odd:  $A^0$ ) and two charged Higgs bosons:  $H^\pm$ . The vector bosons are the photon  $\gamma$ , the  $Z$ -boson  $Z^0$  and the  $W$ -bosons  $W^\pm$ .

The two-body matrix element  $\mathcal{M}_2$  is auto-generated with the help of the FA/FC pack-

ages [20, 21]. The decay width for the processes in Eq. (15) is given by

$$\Gamma(\tilde{G} \rightarrow FX) = \frac{N_c}{16\pi} \frac{\kappa(m_{\tilde{G}}^2, m_F^2, m_X^2)}{m_{\tilde{G}}^3} \frac{1}{4} |\mathcal{M}_2|^2, \quad (16)$$

where  $X = S, V$  and  $N_c$  is the color factor (3 for  $q \tilde{q}$ , 8 for the  $g \tilde{g}$  channel, and 1 otherwise). Please note the factor  $\frac{1}{4}$  being the spin average of the incoming massive gravitino with spin  $\frac{3}{2}$ . As usual, the kinematic function  $\kappa$  is defined as  $\kappa^2(x, y, z) = (x - y - z)^2 - 4yz$ . In parallel, we also calculated these two-body decay processes analytically and included them into `GravitinoPack`. This enables us to cross-check the auto-generated FA/FC code. Details will be published in [25].

### 2.3 Three-body decays

The gravitino decays into a neutralino and a pair of SM particles are

$$\begin{aligned} \tilde{G} &\rightarrow \tilde{\chi}_i^0 \bar{f} f, \\ \tilde{G} &\rightarrow \tilde{\chi}_i^0 VV, \quad VV = Z^0 Z^0, Z^0 \gamma, W^+ W^- \\ \tilde{G} &\rightarrow \tilde{\chi}_i^0 VS, \quad VS = (Z^0, \gamma)(h^0, H^0, A^0), W^+ H^-, W^- H^+ \\ \tilde{G} &\rightarrow \tilde{\chi}_i^0 SS, \quad SS = (h^0, H^0, A^0)(h^0, H^0, A^0), H^+ H^-. \end{aligned} \quad (17)$$

These are 19 three-body decay channels. All possible three-body decay channels for the process  $\tilde{G} \rightarrow \tilde{\chi}_i^0 XY$  are given in Table 1. It is worth to note that  $\tilde{G} \rightarrow \tilde{\chi}_i^0 W^- H^+$  and its charge conjugated process  $\tilde{G} \rightarrow \tilde{\chi}_i^0 W^+ H^-$  count as individual contributions, but  $\Gamma(\tilde{G} \rightarrow \tilde{\chi}_i^0 W^- H^+) = \Gamma(\tilde{G} \rightarrow \tilde{\chi}_i^0 W^+ H^-)$ .

As before, the three-body matrix element  $\mathcal{M}_3$  is auto-generated with the help of the FA/FC packages. The corresponding four-momenta for the decay  $\tilde{G} \rightarrow \tilde{\chi}_i^0 XY$  are fixed by the relation  $k_1 = k_2 + k_3 + k_4$ , where  $X$  and  $Y$  are given in Eq. (17). In our code, the calculation can be performed in three different center of mass systems. This option was used as an additional check for our numerical results. For illustration, we show here only the particular system fixed by the kinematical relation:  $\vec{k}_1 - \vec{k}_2 = \vec{q} = \vec{k}_3 + \vec{k}_4 = 0$ . The Mandelstam variables  $M_1^2$  and  $T$  are defined as

$$\begin{aligned} (k_1 - k_2)^2 &= M_1^2 = (k_3 + k_4)^2, \\ (k_1 - k_3)^2 &= T = (k_2 + k_4)^2. \end{aligned} \quad (18)$$

The decay width for the processes in Eq. (17) is given in differential form by

$$\frac{d^2\Gamma(\tilde{G} \rightarrow \tilde{\chi}_i^0 XY)}{dM_1^2 dT} = \frac{N_c}{256 \pi^3 m_{\tilde{G}}^3} \frac{1}{4} |\mathcal{M}_3|^2. \quad (19)$$

process $\tilde{G} \rightarrow \tilde{\chi}_i^0 XY$	number of graphs	first decay $\tilde{G} \rightarrow \tilde{X}Y$	possible resonances
$\tilde{\chi}_i^0 f \bar{f}$	7	$\tilde{\chi}_i^0(h^0, H^0, A^0, \gamma, Z^0), f \tilde{f}_l^*, \tilde{f}_l \bar{f}$	$h^0, H^0, A^0, Z^0, \tilde{f}_l$
$\tilde{\chi}_i^0 Z^0 Z^0$	4	$\tilde{\chi}_i^0(h^0, H^0), Z^0 \tilde{\chi}_k^0, \tilde{\chi}_k^0 Z^0$	$H^0, \tilde{\chi}_k^0$
$\tilde{\chi}_i^0 Z^0 \gamma$	1	$\tilde{\chi}_k^0 \gamma$	$\tilde{\chi}_k^0$
$\tilde{\chi}_i^0 W^+ W^-$	$6 + 4pt$	$\tilde{\chi}_i^0(h^0, H^0, \gamma, Z^0), W^+ \tilde{\chi}_j^-, \tilde{\chi}_j^+ W^-$	$H^0, \tilde{\chi}_j^\pm$
$\tilde{\chi}_i^0 Z^0 h^0$	$4 + 4pt$	$\tilde{\chi}_i^0(A^0, Z^0), Z^0 \tilde{\chi}_k^0, \tilde{\chi}_k^0 h^0$	$A^0, \tilde{\chi}_k^0$
$\tilde{\chi}_i^0 Z^0 H^0$	$4 + 4pt$	$\tilde{\chi}_i^0(A^0, Z^0), Z^0 \tilde{\chi}_k^0, \tilde{\chi}_k^0 H^0$	$A^0, \tilde{\chi}_k^0$
$\tilde{\chi}_i^0 Z^0 A^0$	$4 + 4pt$	$\tilde{\chi}_i^0(h^0, H^0), \tilde{\chi}_k^0 Z^0, A^0 \tilde{\chi}_k^0$	$H^0, \tilde{\chi}_k^0$
$\tilde{\chi}_i^0 \gamma h^0$	1	$\tilde{\chi}_k^0 \gamma$	$\tilde{\chi}_k^0$
$\tilde{\chi}_i^0 \gamma H^0$	1	$\tilde{\chi}_k^0 \gamma$	$\tilde{\chi}_k^0$
$\tilde{\chi}_i^0 \gamma A^0$	1	$\tilde{\chi}_k^0 \gamma$	$\tilde{\chi}_k^0$
$\tilde{\chi}_i^0 W^+ H^-$	$5 + 4pt$	$\tilde{\chi}_i^0(h^0, H^0, A^0), W^+ \tilde{\chi}_j^-, \tilde{\chi}_j^+ H^-$	$H^0, A^0, \tilde{\chi}_j^\pm$
$\tilde{\chi}_i^0 W^- H^+$	$5 + 4pt$	$\tilde{\chi}_i^0(h^0, H^0, A^0), W^- \tilde{\chi}_j^+, \tilde{\chi}_j^- H^+$	$H^0, A^0, \tilde{\chi}_j^\pm$
$\tilde{\chi}_i^0 h^0 h^0$	4	$\tilde{\chi}_i^0(h^0, H^0), h^0 \tilde{\chi}_k^0, \tilde{\chi}_k^0 h^0$	$H^0, \tilde{\chi}_k^0$
$\tilde{\chi}_i^0 H^0 H^0$	4	$\tilde{\chi}_i^0(h^0, H^0), H^0 \tilde{\chi}_k^0, \tilde{\chi}_k^0 H^0$	$\tilde{\chi}_k^0$
$\tilde{\chi}_i^0 h^0 H^0$	4	$\tilde{\chi}_i^0(h^0, H^0), h^0 \tilde{\chi}_k^0, \tilde{\chi}_k^0 H^0$	$\tilde{\chi}_k^0$
$\tilde{\chi}_i^0 A^0 A^0$	4	$\tilde{\chi}_i^0(h^0, H^0), A^0 \tilde{\chi}_k^0, \tilde{\chi}_k^0 A^0$	$H^0, \tilde{\chi}_k^0$
$\tilde{\chi}_i^0 h^0 A^0$	3	$\tilde{\chi}_i^0(A^0, Z^0), h^0 \tilde{\chi}_k^0$	$\tilde{\chi}_k^0$
$\tilde{\chi}_i^0 H^0 A^0$	3	$\tilde{\chi}_i^0(A^0, Z^0), H^0 \tilde{\chi}_k^0$	$\tilde{\chi}_k^0$
$\tilde{\chi}_i^0 H^+ H^-$	6	$\tilde{\chi}_i^0(h^0, H^0, \gamma, Z^0), H^+ \tilde{\chi}_j^-, \tilde{\chi}_j^+ H^-$	$H^0, \tilde{\chi}_j^\pm$

Table 1: All possible three-body decays channels of the gravitino into a neutralino and a pair of SM particles;  $4pt$  denotes a Feynman graph with four-point interaction, like graph a) in Figure 3. The indices are  $i = 1, \dots, 4$ ;  $k = 2, 3, 4$ ;  $j, l = 1, 2$ .

With  $p^* = \kappa(M_1^2, m_{\tilde{G}}^2, m_{\tilde{\chi}_i^0}^2)/(2M_1)$  and  $k^* = \kappa(M_1^2, m_X^2, m_Y^2)/(2M_1)$ ,  $E_1^2 = m_{\tilde{G}}^2 + p^{*2}$  and  $E_3^2 = m_X^2 + k^{*2}$  we can write the lower and upper bound of  $T$  as

$$T^{\min, \max} = m_{\tilde{G}}^2 + m_X^2 - 2E_1 E_3 \mp 2p^* k^*. \quad (20)$$

We get

$$\Gamma(\tilde{G} \rightarrow \tilde{\chi}_i^0 XY) = \frac{N_c}{256 \pi^3 m_{\tilde{G}}^3} \frac{1}{4} \int_{(m_X + m_Y)^2}^{(m_{\tilde{G}} - m_{\tilde{\chi}_i^0})^2} dM_1^2 \int_{T^{\min}}^{T^{\max}} dT |\mathcal{M}_3|^2. \quad (21)$$

In general, the matrix element  $\mathcal{M}_3$  is a sum of different amplitudes. As in the subsection 2.1, we are using the process  $\tilde{G} \rightarrow \tilde{\chi}_i^0 W^- W^+$  as an example to demonstrate how

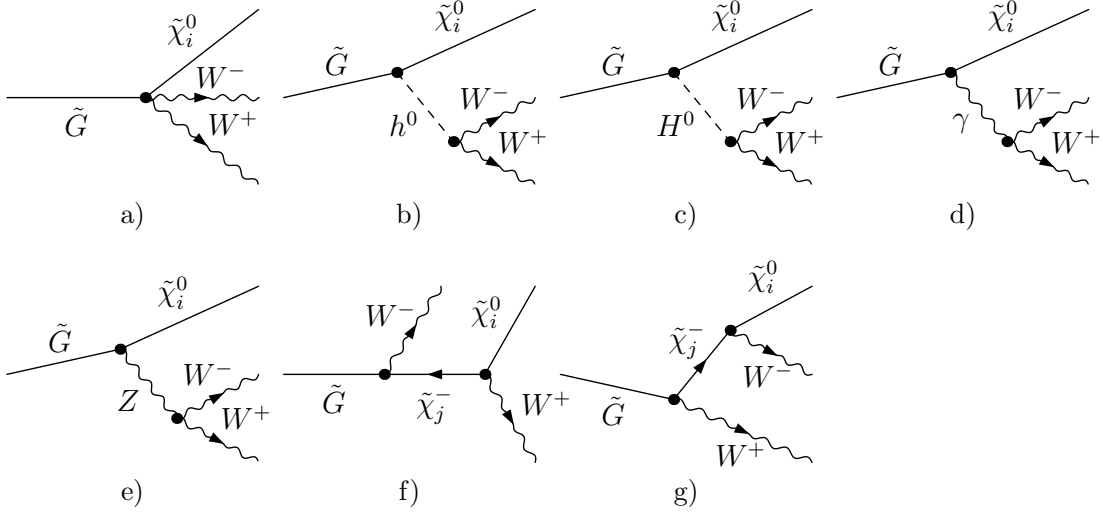


Figure 3: Feynman graphs for the decay  $\tilde{G} \rightarrow \tilde{\chi}_i^0 W^- W^+$ .

one calculates the resonant, the non-resonant and the interference part of Eq. 21. For this particular process there exist 7 Feynman graphs, plotted in Figure 3, which are 9 individual amplitudes. In this case only the  $H^0$  and  $\tilde{\chi}_{1,2}^\pm$  propagators can become resonant. We assume that we have  $H^0$  resonant in  $\mathcal{M}_3^c$ :  $m_{\tilde{G}} > m_{\tilde{\chi}_i^0} + m_{H^0}$  and  $m_{H^0} > 2m_W$ . We write  $\mathcal{M}_3$  as

$$\mathcal{M}_3 = \sum_{i \neq c} \mathcal{M}_3^i + \mathcal{M}_3^c = \mathcal{M}_3^{\text{rest}} + \mathcal{M}_{2,1}(M_1^2) \frac{i}{M_1^2 - m_{H^0}^2 + im_{H^0}\Gamma_{H^0}} \mathcal{M}_{2,2}(M_1^2, T) \quad (22)$$

with  $\mathcal{M}_{2,1} = \mathcal{M}(\tilde{G} \rightarrow \tilde{\chi}_i^0 + H^0)$  and  $\mathcal{M}_{2,2} = \mathcal{M}(H^0 \rightarrow W^- W^+)$  and  $\Gamma_{H^0}$  is the total decay width of  $H^0$ . We get

$$\begin{aligned} |\mathcal{M}_3|^2 &= |\mathcal{M}_3^{\text{rest}}|^2 + |\mathcal{M}_{2,1}|^2 |\mathcal{M}_{2,2}|^2 \frac{1}{(M_1^2 - m_{H^0}^2)^2 + m_{H^0}^2 \Gamma_{H^0}^2} \\ &\quad + 2\text{Re} \left( (\mathcal{M}_3^{\text{rest}})^* \mathcal{M}_{2,1} \mathcal{M}_{2,2} \frac{i(M_1^2 - m_{H^0}^2) + m_{H^0}\Gamma_{H^0}}{(M_1^2 - m_{H^0}^2)^2 + m_{H^0}^2 \Gamma_{H^0}^2} \right). \end{aligned} \quad (23)$$

We use

$$\lim_{m\Gamma \rightarrow 0} \left( \frac{1}{(s - m^2)^2 + m^2 \Gamma^2} \right) = \frac{\pi}{m\Gamma} \delta(s - m^2) \quad (24)$$

and apply the narrow width approximation (NWA) for  $H^0$ ,  $\Gamma_{H^0} \ll m_{H^0}$ . We have three terms in Eq. (23). The first one,  $\Gamma^{\text{non-reso}}$ , leads to the remaining non-resonant three-body decay width. To get this, we just have to substitute  $\mathcal{M}_3$  in Eq. (21) by  $\mathcal{M}_3^{\text{rest}}$ . The second

one corresponds to the resonant part. Using  $dT = 2p^*k^*d\cos\theta$  and  $M_1^2 \rightarrow m_{H^0}^2$  we get

$$\Gamma^{\text{reso}}(\tilde{G} \rightarrow \tilde{\chi}_i^0 W^- W^+) = \frac{1}{4} \frac{1}{128 \pi^3 m_{\tilde{G}}^3} \frac{\pi}{m_{H^0} \Gamma_{H^0}} p^* k^* |\mathcal{M}_{2,1}|^2 \int_{-1}^1 d\cos\theta |\mathcal{M}_{2,2}|^2. \quad (25)$$

$\mathcal{M}_{2,2}$  must be independent on  $\cos\theta$  because  $H^0$  is at rest. Using Eq. (16) we have

$$\Gamma(\tilde{G} \rightarrow \tilde{\chi}_i^0 H^0) = \frac{1}{4} \frac{m_{H^0}}{8\pi} \frac{p^*}{m_{\tilde{G}}^3} |\mathcal{M}_{2,1}|^2 \quad \text{and} \quad \Gamma(H^0 \rightarrow W^- W^+) = \frac{1}{8\pi} \frac{k^*}{m_{H^0}^2} |\mathcal{M}_{2,2}|^2. \quad (26)$$

Note that  $(m_{H^0}/m_{\tilde{G}})p^* = \kappa(m_{\tilde{G}}^2, m_{H^0}^2, m_{\tilde{\chi}_i^0}^2)/(2m_{\tilde{G}})$  is the momentum of the outgoing particles in the restframe of the gravitino. We can write Eq. (25) as

$$\Gamma^{\text{reso}}(\tilde{G} \rightarrow \tilde{\chi}_i^0 W^- W^+) = \Gamma(\tilde{G} \rightarrow \tilde{\chi}_i^0 H^0) \frac{\Gamma(H^0 \rightarrow W^- W^+)}{\Gamma_{H^0}}. \quad (27)$$

The third term in Eq. (23) denotes the interference. It can be written in the NWA as

$$\Gamma^{\text{if}}(\tilde{G} \rightarrow \tilde{\chi}_i^0 W^- W^+) = \frac{1}{4} \frac{1}{64\pi^2 m_{\tilde{G}}^3} p^* k^* \int_{-1}^1 d\cos\theta \text{Re}((\mathcal{M}_3^{\text{rest}})^* \mathcal{M}_{2,1} \mathcal{M}_{2,2}). \quad (28)$$

We can generalize our formulas to include  $n$  resonances, for example, see the last column in Table 1. The total matrix element is a sum of non-resonant and a sum of resonant matrix elements. The sum of the non-resonant matrix elements is denoted as before as  $\mathcal{M}_3^{\text{rest}}$ . Moreover, we split the sum of the resonant matrix elements,  $\mathcal{M}_3^n$ , into the matrix element with the particular resonance  $j$ ,  $\mathcal{M}_3^j$ , and the other ones,  $\mathcal{M}_3^{!j} = \sum_{k \neq j} \mathcal{M}^k$ . The result for the non-resonant part is the same like in the case with only one resonance. The resonant part is

$$\Gamma^{\text{reso}}(\tilde{G} \rightarrow \tilde{\chi}_i^0 XY) = \frac{1}{512 \pi^2 m_{\tilde{G}}^3} \sum_j \frac{p^* k^*}{m_j \Gamma_j} |\mathcal{M}_{2,1}^j|^2 \int_{-1}^1 d\cos\theta |\mathcal{M}_{2,2}^j|^2, \quad (29)$$

and the interference term reads

$$\Gamma^{\text{if}}(\tilde{G} \rightarrow \tilde{\chi}_i^0 XY) = \frac{1}{256 \pi^2 m_{\tilde{G}}^3} \sum_j p^* k^* \int_{-1}^1 d\cos\theta \text{Re} \left[ \left( \mathcal{M}_3^{\text{rest}} + \frac{1}{2} \mathcal{M}_3^{!j} \right)^* \mathcal{M}_{2,1}^j \mathcal{M}_{2,2}^j \right]. \quad (30)$$

The factor 1/2 in front of  $\mathcal{M}_3^{!j}$  is necessary in order to avoid double counting of the interference terms within  $|\mathcal{M}_3^n|^2$ . These NWA formulas, Eqs. (29) and (30), are only applicable when there is no overlap of resonances,  $\Gamma_j + \Gamma_k \ll |m_j - m_k|$  for all possible couples of  $j$  and  $k$ .

### 3 Numerical results

In our numerical analysis we choose representative points from various supersymmetric models, assuming different mechanism for the supersymmetry breaking. In particular, we study points based on the pMSSM [31], the CMSSM [32,33] model and the NUHM [34]. These points satisfy the sparticle mass bounds from LHC [35] and the cosmological constraints on the amount of the dark matter as measured by the WMAP [36] and Planck [37] experiments, assuming that the dark matter is made of neutralinos. In addition, we use the branching ratio for the process  $B_s \rightarrow \mu^+ \mu^-$  as it is measured from LHCb and other experiments [38, 39], Higgs mass at  $\sim 126$  GeV [40], and the recent XENON100 [41] direct detection bound.

Parameters	Coannihilation point	$A^0$ -funnel point
$\tan \beta = \langle H_2^0 \rangle / \langle H_1^0 \rangle$	30	20
$\mu$ , Higgsino mixing parameter	2200 GeV	700 GeV
$M_A$ , $A^0$ Higgs boson mass	1100 GeV	770 GeV
$(M_1, M_2, M_3)$ , Gauginos masses	(399,1000,3000) GeV	(400,800,2400) GeV
$A_t$ , top trilinear coupling	-2300 GeV	-2050 GeV
$A_b$ , bottom trilinear coupling	-2300 GeV	-2050 GeV
$A_\tau$ , tau trilinear coupling	-2300 GeV	-1000 GeV
$m_{\tilde{q}_L}$ , 1st/2nd family $Q_L$ squark mass	1500 GeV	1500 GeV
$m_{\tilde{u}_R}$ , 1st/2nd family $U_R$ squark	1500 GeV	1500 GeV
$m_{\tilde{d}_R}$ , 1st/2nd family $D_R$ squark	1500 GeV	1500 GeV
$m_{\tilde{\ell}_L}$ , 1st/2nd family $L_L$ slepton	800 GeV	600 GeV
$m_{\tilde{e}_R}$ , 1st/2nd family $E_R$ slepton	2500 GeV	2500 GeV
$m_{\tilde{Q}_{3L}}$ , 3rd family $Q_L$ squark	1100 GeV	800 GeV
$m_{\tilde{t}_R}$ , 3rd family $U_R$ squark	1100 GeV	1000 GeV
$m_{\tilde{b}_R}$ , 3rd family $D_R$ squark	1100 GeV	1500 GeV
$m_{\tilde{L}_{3L}}$ , 3rd family $L_L$ slepton	400 GeV	800 GeV
$m_{\tilde{\tau}_R}$ , 3rd family $E_R$ slepton	2000 GeV	2000 GeV

Table 2: The pMSSM parameters used as input for the two points studied in our analysis.

As discussed in the previous section, the total three-body decay result consists of three parts: the resonant part calculated, the non-resonant part, and the interference term.

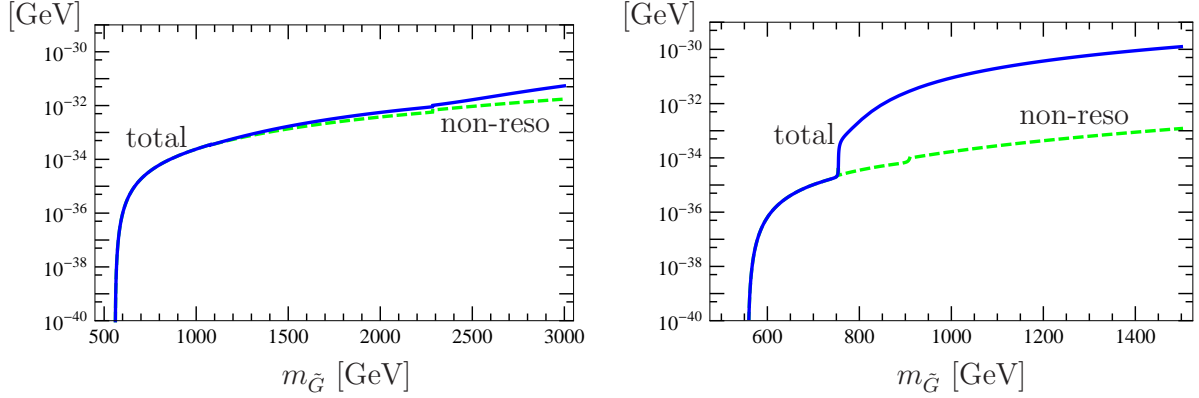


Figure 4: The decay width for the process  $\tilde{G} \rightarrow \tilde{\chi}_1^0 W^+ W^-$  left (right), for the stau-coannihilation ( $A^0$ -funnel) pMSSM point as discussed in the text. The solid blue line is the total width (resonant and non-resonant part) of this decay, while the dashed green line is the non-resonant part only.

The resonant part, naturally, vanishes below the threshold of the on-shell production of the intermediate particle. The interference term is numerically always very small in the studied scenarios and negligible compared to the non-resonant and resonant parts. Therefore, we will not show explicitly this term in the figures with three-body gravitino decays.

First we study two pMSSM points, one in the stau-coannihilation region ( $m_{\tilde{\tau}_1} \simeq m_{\tilde{\chi}_1^0}$ ), and the other one in the  $A^0$ -funnel region ( $m_{A^0} \simeq 2m_{\tilde{\chi}_1^0}$ ), with the input parameters given in Table 2. At the former point, we get a neutralino dark matter relic density compatible with WMAP data by increasing the neutralino pair annihilation cross-section by adding  $\tilde{\chi}_1^0\text{-}\tilde{\tau}_1$  coannihilation processes, while at the latter one by using the rapid pair annihilation of the  $\tilde{\chi}_1^0$ 's through the  $A^0$  resonant exchange. For the coannihilation point we get the masses  $m_{\tilde{\chi}_{1,2,3,4}^0} = (399, 998, 2201, 2203)$  GeV,  $m_{\tilde{\chi}_{1,2}^+} = (998, 2203)$  GeV, and  $m_{H^+} = 1103$  GeV. For the funnel point we get  $m_{\tilde{\chi}_{1,2,3,4}^0} = (397, 675, 703, 830)$  GeV,  $m_{\tilde{\chi}_{1,2}^+} = (674, 830)$  GeV, and  $m_{H^+} = 774$  GeV. These values will help us understand the various features appearing in the figures be discussed below.

In Figure 4 left, the decay width for the processes  $\tilde{G} \rightarrow \tilde{\chi}_1^0 W^+ W^-$  is shown. The solid blue line is the total width (resonant and non-resonant part), while the dashed green line is the non-resonant part only. As can be seen in Table 1, for this three-body decay channel, we can have a resonant behavior through the chargino ( $\tilde{\chi}_{1,2}^+$ ) or  $H^0$  exchange. This means, that for a gravitino mass  $m_{\tilde{G}} = m_{\tilde{\chi}_j^+} + M_W$  and  $m_{\tilde{G}} = m_{\tilde{\chi}_1^0} + m_{H^0}$ , one expects to see a structure, being proportional to the resonant contribution as given in

Eq. (29), following the NWA. The size of the NWA term, for example in the case of the  $\tilde{\chi}_1^+$  resonance, is proportional to the partial width  $\tilde{\chi}_1^+ \rightarrow \tilde{\chi}_1^0 W^+$ , and inversely proportional to the total width of  $\tilde{\chi}_1^+$ . In Figure 4 left, there are very small structures that correspond to chargino thresholds  $m_{\tilde{G}} = m_{\tilde{\chi}_{1,2}^+} + M_W$ . For this case the total chargino widths are  $\Gamma_{\tilde{\chi}_{1,2}^+} = (8, 144)$  GeV. The partial chargino width to  $\tilde{\chi}_1^0 W^+$  is of the order  $10^{-4}$  GeV because  $\tilde{\chi}_1^0$  is almost a pure bino state, and for a chargino-neutralino- $W$  interaction one needs a wino-wino or a higgsino-higgsino combination of chargino-neutralino. Thus the effects are suppressed in this scenario. In Figure 4 right, we show the corresponding widths for the  $A^0$ -funnel point. For this point we have the total widths  $\Gamma_{\tilde{\chi}_{1,2}^+} = (0.7, 5)$  GeV, and the partial width  $\tilde{\chi}_1^+ \rightarrow \tilde{\chi}_1^0 W^+$  is almost three orders of magnitude bigger ( $\mathcal{O}(0.1)$  GeV) because the charginos are mixed states of gauginos and higgsinos and  $\tilde{\chi}_1^0$  is again a bino state but with non-negligible admixtures of higgsinos and winos. This makes the partial gravitino width quite large after the  $\tilde{\chi}_1^+ W^-$  threshold.

Before we discuss other gravitino decay channels some comments are in order. First, it is important to note that below the first threshold (the  $\tilde{\chi}_1^+$  for this case) the knowledge of the full three-body amplitude is important in the computation of the gravitino decay width. Looking at Figure 4 one notices that the size of the width below and above the threshold is comparable, especially for the coannihilation point. Thus, using only the two body decays (or the NWA terms) one gets, in general, inadequate results. A second comment is related to the relative size of the resonant and the non-resonant contributions. If the partial width of the intermediate unstable particle, like the  $\tilde{\chi}_1^+ \rightarrow \tilde{\chi}_1^0 W^+$  at the coannihilation point, is small these two contributions are comparable. In this case the non-resonant contribution dominates and therefore in Figure 4 left the blue and the green curves are very close. For example, in Figure 4 left at  $m_{\tilde{G}} = 2$  TeV we get  $\Gamma^{\text{reso}} = 1.8 \times 10^{-33}$  GeV and  $\Gamma^{\text{non-reso}} = 3.8 \times 10^{-33}$  GeV. This underlines the relevance of the full three-body calculation.

We now turn to Figure 5, where we display the width for the channel  $\tilde{G} \rightarrow \tilde{\chi}_1^0 Z^0 Z^0$ . In this case, the possible resonant particles, as can be seen in Table 1, are the heavier neutralinos  $\tilde{\chi}_{2,3,4}^0$  and the heavy  $CP$ -even Higgs boson  $H^0$ . The first kink in Figure 5 left (coannihilation point) corresponds to the threshold of the two body process  $\tilde{G} \rightarrow \tilde{\chi}_2^0 Z^0$ , where  $m_{\tilde{\chi}_2^0} = 998$  GeV. The corresponding increase in Figure 5 right, for  $m_{\tilde{\chi}_2^0} = 675$  GeV, is much stronger because the partial width for the channel  $\tilde{\chi}_2^0 \rightarrow \tilde{\chi}_1^0 Z^0$  is three order of magnitudes bigger, while the total width  $\Gamma_{\tilde{\chi}_2^0}$  is almost ten times smaller. For a neutralino-neutralino- $Z$  interaction both neutralino states must have a higgsino component. As already stated, in the coannihilation scenario the lightest neutralino is almost a pure bino

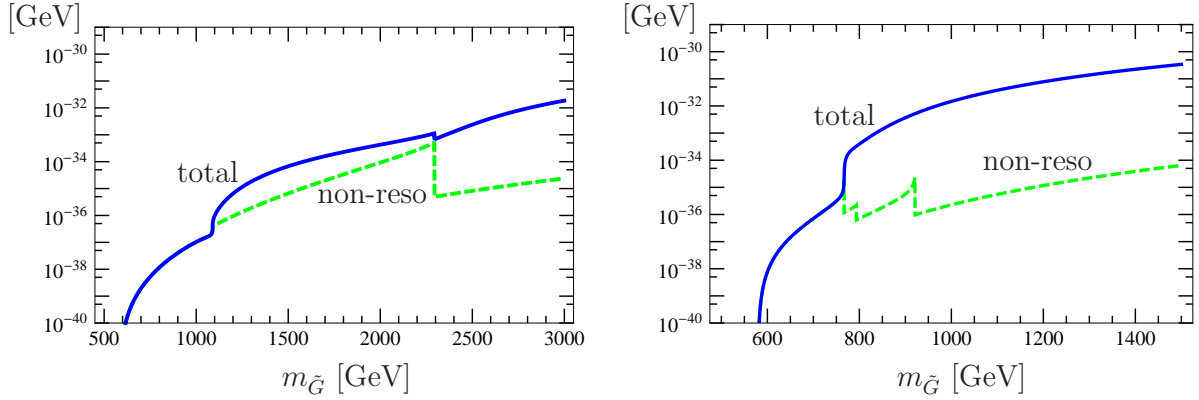


Figure 5: The decay width for the process  $\tilde{G} \rightarrow \tilde{\chi}_1^0 Z^0 Z^0$  left (right), for the stau-coannihilation ( $A^0$ -funnel) pMSSM point as discussed in the text. The lines are as in Figure 4.

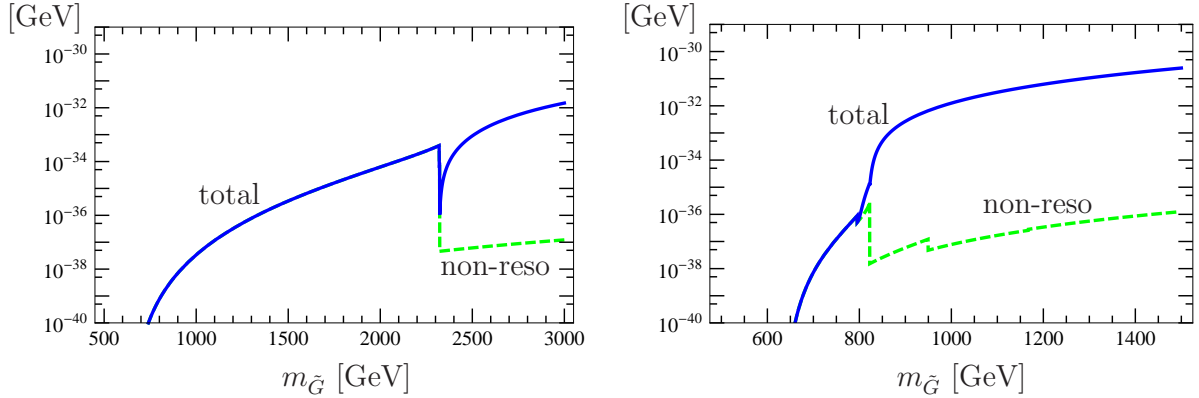


Figure 6: The decay width for the process  $\tilde{G} \rightarrow \tilde{\chi}_1^0 h^0 h^0$  left (right), for the stau-coannihilation ( $A^0$ -funnel) pMSSM point as discussed in the text. The lines are as in Figure 4.

state which suppresses the  $\tilde{\chi}_2^0 \rightarrow \tilde{\chi}_1^0 Z^0$  coupling. In addition, the effects of the thresholds of the neutralinos  $\tilde{\chi}_{3,4}^0$  with masses 702 and 829 GeV (see Figure 5 right), can be seen also in the dashed line denoting the non-resonant contribution.

In Figure 6, we study the channel  $\tilde{G} \rightarrow \tilde{\chi}_1^0 h^0 h^0$ . The possible resonant exchanged particles are the same as in  $\tilde{G} \rightarrow \tilde{\chi}_1^0 Z^0 Z^0$ , namely the heavier neutralinos  $\tilde{\chi}_{2,3,4}^0$  and the heavy  $CP$ -even Higgs boson  $H^0$ . In the coannihilation point (left) the effect of the enhancement after the threshold of the  $\tilde{\chi}_2^0$  resonance at  $m_{\tilde{G}} \sim 1100$  GeV is quite suppressed, because the  $\tilde{\chi}_2^0 \rightarrow \tilde{\chi}_1^0 h^0$  partial width is small as the  $\tilde{\chi}_2^0 \rightarrow \tilde{\chi}_1^0 Z^0$  before. On the other hand, the  $\tilde{\chi}_{3,4}^0 \rightarrow \tilde{\chi}_1^0 h^0$  widths are much bigger, producing this large structure in the gravitino decay width across the almost degenerate  $\tilde{\chi}_{3,4}^0$  thresholds at  $m_{\tilde{G}} \sim 2300$  GeV. At the

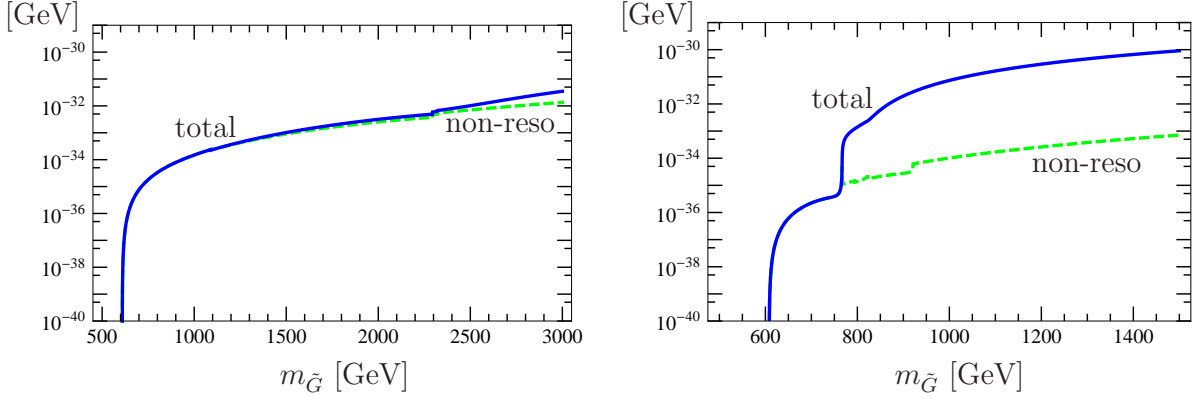


Figure 7: The decay width for the process  $\tilde{G} \rightarrow \tilde{\chi}_1^0 Z^0 h^0$  left (right), for the stau-coannihilation ( $A^0$ -funnel) pMSSM point as discussed in the text. The lines are as in Figure 4.

$A^0$ -funnel point the situation is different. The threshold effect across the  $\tilde{\chi}_2^0$  resonance at  $m_{\tilde{G}} = 801$  GeV is much bigger due to the larger  $\tilde{\chi}_2^0 \rightarrow \tilde{\chi}_1^0 h^0$  decay width. Moreover, the thresholds of the heavier neutralinos are also visible.

Figure 7 shows the width for the decay  $\tilde{G} \rightarrow \tilde{\chi}_1^0 Z^0 h^0$  as a function of  $m_{\tilde{G}}$ . As in Figure 4, the effect of the thresholds is not important for the coannihilation point (left). In contrast, especially the  $\tilde{\chi}_2^0$  threshold can be seen at the  $A^0$ -funnel point (right). Note again, that at the coannihilation point (left)  $\tilde{\chi}_1^0$  is a pure bino state. Therefore, the decays  $\tilde{\chi}_{2,3,4}^0 \rightarrow \tilde{\chi}_1^0 Z^0$  are suppressed and the non-resonant contribution is dominant.

Closing the discussion on the gravitino widths at these two representative pMSSM points, we show in Figure 8 the three-body decay widths of the gravitino decaying into  $\tilde{\chi}_1^0$  together with  $q\bar{q}$ ,  $\bar{l}l$ , and  $W$ ,  $Z$ -boson pairs at the  $A^0$ -funnel point. We also show the two-body decay channel  $\tilde{G} \rightarrow \tilde{\chi}_1^0 \gamma$  as a reference, because it is dominant for small  $m_{\tilde{G}}$ . In the left figure we also show  $\Gamma^{\text{total}}$  which is the full two-body width plus the sum of the non-resonant part of three-body decay widths with  $\tilde{\chi}_1^0$ , denoted by “total”. In the right figure we show the relative quantities in terms of  $\Gamma^{\text{total}}$ ;  $q\bar{q}$  stands for the sum over all six quark flavors,  $\sum_{i=1,6} \Gamma^{\text{reso} + \text{non-reso}}(\tilde{G} \rightarrow \tilde{\chi}_1^0 q_i \bar{q}_i)$  and  $\bar{l}l$ ,  $q_i = u, d, c, s, t, b$ , and  $\bar{l}l$  the sum of the three charged lepton and three neutrino flavors,  $\sum_{j=1,3} \left( \Gamma^{\text{non-reso} + \text{reso}}(\tilde{G} \rightarrow \tilde{\chi}_1^0 l_j^+ l_j^-) + \Gamma^{\text{non-reso} + \text{reso}}(\tilde{G} \rightarrow \tilde{\chi}_1^0 \nu_{l_j} \bar{\nu}_{l_j}) \right)$ ,  $l_j = e, \nu, \tau$ . The decay width summing up the decays into all fermion pair can reach 38%, into the  $W$ -boson pair 5.6% and into the  $Z$ -boson pair 1.5% in the shown range. The analogous plots for the coannihilation point look similar but the decays into  $W$ - and  $Z$ -boson pairs are suppressed by about two orders of magnitude due to the pure bino state of the LSP as already discussed before.

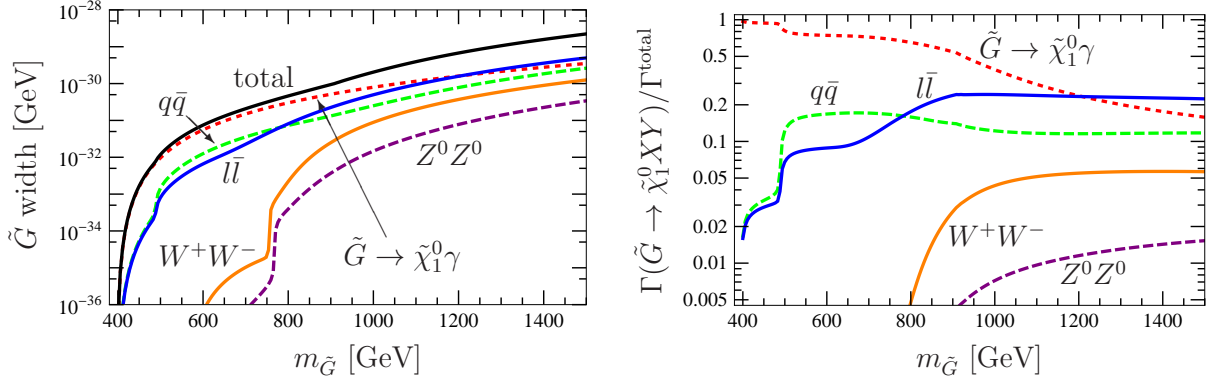


Figure 8: The three-body decay widths of the gravitino decaying into  $\tilde{\chi}_1^0$  and  $q\bar{q}$ ,  $l\bar{l}$ ,  $W$ -pairs, and  $Z$ -pairs at the  $A^0$ -funnel point; “total” denotes  $\Gamma^{\text{total}}$  which is the full two-body width plus the sum of the non-resonant part of three-body decay widths with  $\tilde{\chi}_1^0$ ;  $q\bar{q}$  stands for the sum over all six quark flavors and  $l\bar{l}$  for the sum over the three charged lepton and three neutrino flavors. The red dotted lines denote the two-body decay  $\tilde{G} \rightarrow \tilde{\chi}_1^0 \gamma$ . In the right figure we display the corresponding branching ratios for the decay channels plotted in the left figure.

In addition to these two pMSSM points, we study two other representative points: one based on the CMSSM and another based on the NUHM. The CMSSM is characterized by five parameters: the universal soft mass for scalar particles  $m_0$ , the universal soft gaugino mass  $m_{1/2}$ , the universal trilinear coupling  $A_0$ , the ratio of the two vacuum expectation values of the Higgs doublets  $\tan \beta = \frac{v_2}{v_1}$  and the sign of the Higgsino mixing mass  $\mu$ . In the so-called NUHM1 model [42] there is one extra free parameter, the soft mass of the Higgs doublets. In our analysis, this mass is fixed by the absolute value of the Higgsino mixing mass  $\mu$  at the electro-weak symmetry breaking scale, that we use as input parameter. The values of the parameters  $m_0$ ,  $m_{1/2}$  and  $A_0$  for both models are defined at the GUT scale.

The CMSSM point we are using is defined as:  $m_0 = 1150$  GeV,  $m_{1/2} = 1115$  GeV,  $\tan \beta = 40$ ,  $A_0 = -2.5 m_0 = -2750$  GeV and  $\text{sign}(\mu) > 0$ . Using the package `SPheno` [43] this point yields  $m_h \simeq 126$  GeV. Quite similar results are obtained by using the `FeynHiggs` package [44]. Furthermore, this point is compatible with the WMAP bound on the neutralino relic density and it delivers acceptable values for the decay  $B_s \rightarrow \mu^+ \mu^-$  and the dark matter direct detection cross-section. This point belongs to the stau-coannihilation region of the CMSSM and has been discussed in [45]. On the other hand, the NUHM1 point is defined as  $m_0 = 1000$  GeV,  $m_{1/2} = 1200$  GeV,  $\tan \beta = 10$ ,  $A_0 = -2.5 m_0 = -2500$  GeV and  $\mu = 500$  GeV. At this point the light Higgs mass is  $m_h = 126.5$  GeV and it is also compatible with other cosmological and accelerator constraints [42].

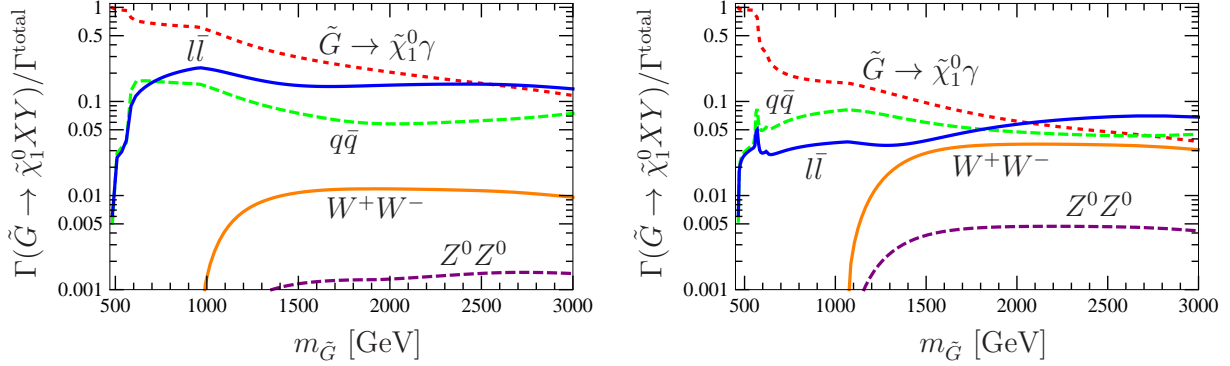


Figure 9: The branching ratios for the CMSSM (left) and NUHM point (right). The curves are as in Figure 8 right.

In Figure 9 we present the various branching ratios for the important gravitino decay channels, as functions of the gravitino mass, as we have done in Figure 8 right. At the CMSSM point the four neutralino masses are  $m_{\tilde{\chi}_{1,2,3,4}^0} = (485, 919, 1824, 1826)$  GeV. The  $\tilde{\chi}_1^0$  is almost a pure bino with its higgsino components less than 0.1%. We notice that the branching ratios for the channels  $\tilde{\chi}_1^0 l \bar{l}$  and  $\tilde{\chi}_1^0 q \bar{q}$  are approximately of the order of 10% after the mass threshold of the 500 GeV. The two-body channel  $\tilde{\chi}_1^0 \gamma$  clearly dominates in the range of small gravitino masses, but after 2000 GeV it becomes comparable to the  $\tilde{\chi}_1^0 l \bar{l} / q \bar{q}$  channels. On the other hand, the branching ratio for the  $\tilde{\chi}_1^0 W^+ W^-$  channel is almost an order of magnitude smaller, and for the channel  $\tilde{\chi}_1^0 Z^0 Z^0$  a further order of magnitude smaller.

Figure 9 right displays the branching ratios for the NUHM point. At this point  $m_{\tilde{\chi}_{1,2,3,4}^0} = (470, 511, 539, 1025)$  GeV and there  $\tilde{\chi}_1^0$  has a significant higgsino component. The two higgsino components ( $\tilde{H}_{1,2}^0$ ) of the LSP amount to approximately 25% each. In comparison to the CMSSM point, the bino component decreased from almost 100% to about 50%. The wino component of  $\tilde{\chi}_1^0$  is very small. Therefore, the channels which couple to the bino and wino components, like  $\tilde{\chi}_1^0 l \bar{l} / q \bar{q}$  except that with stops, are suppressed by a factor of 2 or more, in comparison to the CMSSM case. The channels that depend on the higgsino content of  $\tilde{\chi}_1^0$ , like  $\tilde{\chi}_1^0 W^+ W^- / Z^0 Z^0$  are enhanced by approximately a factor of 2. For both the CMSSM and NUHM cases displayed in Figure 9, the not shown two-body channels, as  $\tilde{\chi}_j^+ W^-$ ,  $\tilde{\chi}_i^0 Z^0$  and  $\tilde{g} g$ , provide the bulk of the remaining contribution to the total gravitino decay width. We notice that also in this case for  $m_{\tilde{G}} \gtrsim 2000$  GeV the channels  $\tilde{\chi}_1^0 l \bar{l} / q \bar{q}$  are comparable to the two-body channel  $\tilde{\chi}_1^0 \gamma$ .

In Figure 10 we present the ratio  $\Gamma^{\text{non-reso}}(\tilde{G} \rightarrow \tilde{\chi}_1^0 X Y) / \Gamma^{2B}$  (green solid curve) and

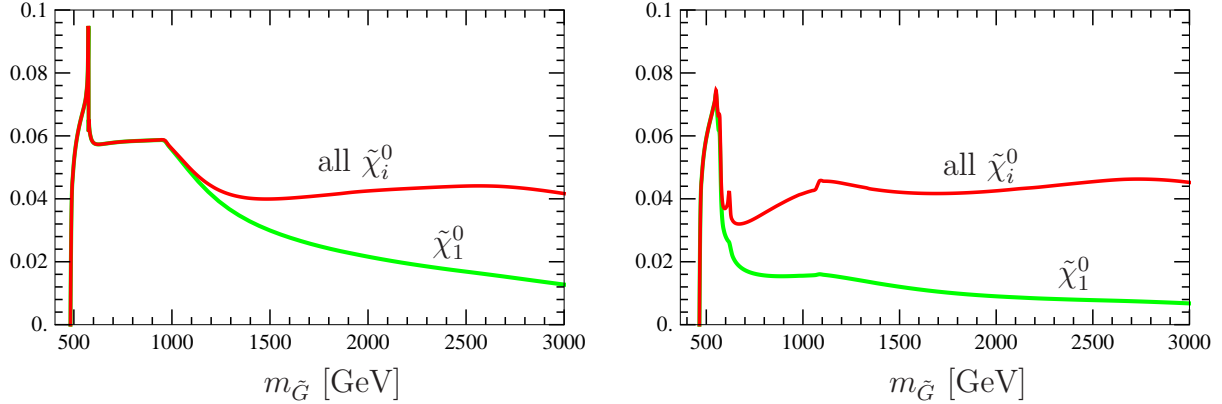


Figure 10: The ratio  $\Gamma^{\text{non-reso}}(\tilde{G} \rightarrow \tilde{\chi}_1^0 X Y)/\Gamma^{2B}$  (green curve) and  $\sum_{i=1,\dots,4} \Gamma^{\text{non-reso}}(\tilde{G} \rightarrow \tilde{\chi}_i^0 X Y)/\Gamma^{2B}$  (red curve), for the CMSSM (left) and NUHM (right) point.  $\Gamma^{2B}$  is the total gravitino two-body decay width.

the  $\sum_{i=1,\dots,4} \Gamma^{\text{non-reso}}(\tilde{G} \rightarrow \tilde{\chi}_i^0 X Y)/\Gamma^{2B}$  (red solid curve) as function of the gravitino mass for the CMSSM (left) and NUHM (right) point, we discussed before.  $\Gamma^{2B}$  denotes the total two-body width of the gravitino. These figures give us an idea of the contribution of the heavier neutralino states in comparison to  $\tilde{\chi}_1^0$ , especially for the non-resonant contribution of the three-body decay channels  $\tilde{\chi}_i^0 X Y$ . The spikes in both cases, just before  $m_{\tilde{G}} = 600$  GeV are due to the threshold of the two-body decay  $\tilde{G} \rightarrow \tilde{\chi}_1^0 Z^0$ . Especially for the NUHM case at right, the second smaller spike corresponds to the almost degenerate threshold for the processes  $\tilde{G} \rightarrow \tilde{\chi}_{2,3}^0 Z^0$ . The structures in the region  $m_{\tilde{G}} \simeq 1000$  GeV correspond to threshold  $\tilde{G} \rightarrow \tilde{\chi}_2^0 Z^0$ , for the CMSSM case and to  $\tilde{G} \rightarrow \tilde{\chi}_4^0 Z^0$  for NUHM.

We see that for  $m_{\tilde{G}}$  at 3 TeV the ratio  $\sum_{i=1,\dots,4} \Gamma^{\text{non-reso}}(\tilde{G} \rightarrow \tilde{\chi}_i^0 X Y)/\Gamma^{2B}$  is four times larger than the ratio  $\Gamma^{\text{non-reso}}(\tilde{G} \rightarrow \tilde{\chi}_1^0 X Y)/\Gamma^{2B}$ , both for the CMSSM and the NUHM point. On the other hand, for the CMSSM point for  $m_{\tilde{G}}$  up to 1 TeV the ratio  $\Gamma^{\text{non-reso}}(\tilde{G} \rightarrow \tilde{\chi}_1^0 X Y)/\Gamma^{2B}$  dominates over the other neutralino contributions. For the NUHM point (right figure) the dominance of the  $\tilde{\chi}_1^0$  ends just before  $m_{\tilde{G}} = 600$  GeV. Furthermore, from Figure 10 one can see the size of the total non-resonant contribution of the three-body decay channel  $\tilde{G} \rightarrow \tilde{\chi}_i^0 X Y$  relative to the dominant two-body decay width. For the CMSSM (NUHM) point, in the region up to  $m_{\tilde{G}} \lesssim 1$  TeV (650 GeV) the non-resonant part of the three-body decays into  $\tilde{\chi}_1^0$  is about 6% and decreases to 2% (1%) for  $m_{\tilde{G}} > 2$  TeV.

An important comment, however, is in order. The numerical smallness of the contribution of the non-resonant three-body decay width can be misinterpreted to consider

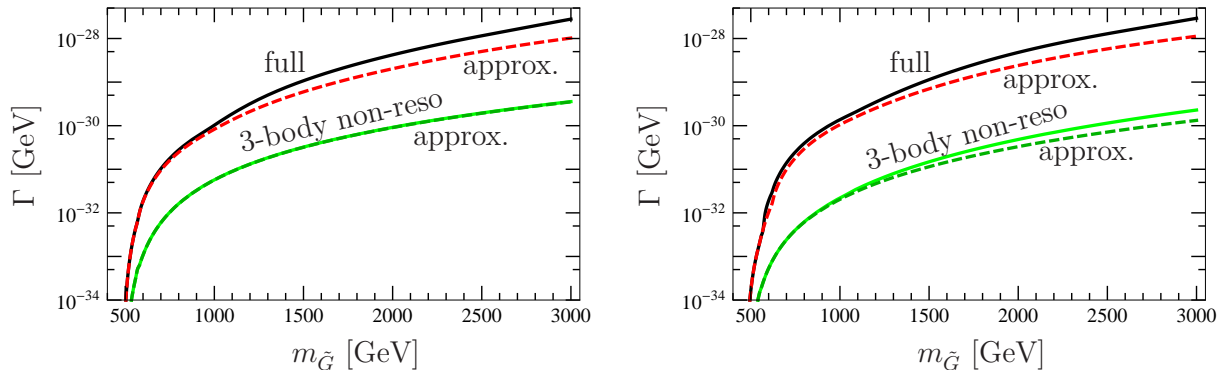


Figure 11: Comparison between the full gravitino width, that is the contribution from the two-body decays and the three-body non-resonant part (black curve) and the approximation (red dashed curve). The green curve is the three-body non-resonant part only and the dark green dashed curve the corresponding approximation. The left (right) figure correspond to the CMSSM (NUHM) point as described in the text.

the three-body decays to be as unimportant in comparison to the two-body decays. Discussing the details of various individual three-body channels in the Figures 4–7 we have seen that below the two-body mass thresholds, the exact knowledge of the gravitino three-body decay widths is important in the calculation of the corresponding branching ratios in the whole range of  $m_{\tilde{G}}$ . Thus, it is essential to calculate *all* possible three-body decay channels for the process  $\tilde{G} \rightarrow \tilde{\chi}_i^0 X Y$ , in order to have the complete information both for the total gravitino width and the individual branching ratios, for any gravitino mass.

In Figure 11 we compare the full result for the gravitino decay width (black curve), that corresponds to the sum of the two-body decays and the non-resonant part of the three-body decays  $\tilde{G} \rightarrow \tilde{\chi}_i^0 X Y$ , with a commonly used approximation (red dashed curve). In this approximation one calculates the gravitino width using the two-body channels  $\tilde{\chi}_i^0(\gamma, Z^0, h^0, H^0, A^0)$  and the three-body channels  $\tilde{\chi}_1^0 f \bar{f}$ , where  $f$  can be either lepton or quark. The approximation is relatively good up to  $m_{\tilde{G}} = 1000$  GeV, differing from the full result by  $\sim 20\%$ , for the CMSSM point. For the NUHM point this difference is  $\sim 25\%$ . But for larger gravitino masses ( $m_{\tilde{G}} \simeq 3000$  GeV), where almost all two-body channels contribute the difference is quite important. The approximation underestimates the full result by a factor of 2.7 for the CMSSM point and by 2.9 for the NUHM. Comparing the non-resonant contribution of the three-body decays we get a different picture. For the CMSSM point, the approximation (dark green dashed curve) describe quite well the full non-resonant part (light green solid curve). The reason for this is that the dominant bino content of  $\tilde{\chi}_1^0$  leads to the dominance of the three-body decay channel  $\tilde{\chi}_1^0 f \bar{f}$ , as

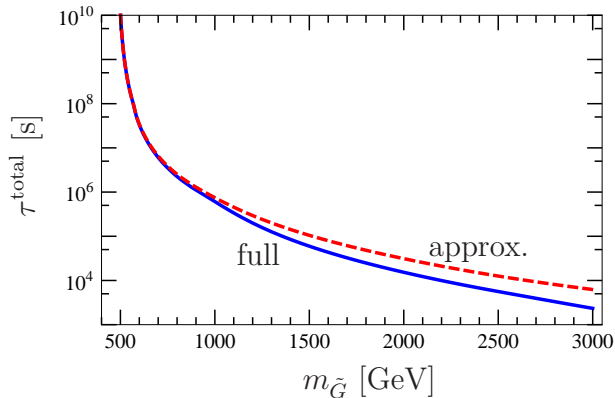


Figure 12: The gravitino lifetime as a function of the gravitino mass for the CMSSM point. The blue curve is the lifetime as calculated including all the two-body and three-body channels in our study and the red dashed curve corresponds to the approximation described in the text to Figure 11.

we have seen also in Figure 9. On the other hand, at the NUHM point the approximations are equally important, the approximation is almost a factor of 2 smaller than the complete result for  $m_{\tilde{G}} = 3$  TeV. This is due to the fact that the three-body channels  $\tilde{\chi}_1^0 W^+ W^- / Z^0 Z^0$  etc. are not included in the approximation but play an important role in this scenario.

The relevance of the calculation of the full three-body gravitino decay width is also underlined in Figure 12. For the CMSSM point, we display the gravitino lifetime in seconds using the full result (blue curve) and the approximation described above (red dashed curve). The corresponding figure for the NUHM point is quite similar. Reflecting the behavior of Figure 11 the approximation up to  $m_{\tilde{G}} = 1$  TeV is relatively good, but for larger gravitino masses overestimates the gravitino lifetime by a factor of 2 and more. As already mentioned, the precise calculation of the gravitino lifetime especially in the range  $m_{\tilde{G}} \sim 2-4$  TeV, is important because one thinks that the models with unstable gravitinos can explain the so-called Lithium cosmological puzzle [15]. This is due to the fact that the lifetime of the gravitino for these gravitino masses is  $\sim 10^4$  s and shorter, time scales that can be quite relevant to BBN predictions for the primordial light elements abundances, and especially for the  ${}^6\text{Li}$  and  ${}^7\text{Li}$  isotopes. Thus, our calculation is of importance in the phenomenology of supersymmetric models with unstable gravitinos.

The use of the Weyl-van-der-Waerden formalism for the calculation of the gravitino width allows one to explicitly compute the individual contributions of the four gravitino spin states to the total width. It is known that the gravitino in broken supersymmetric

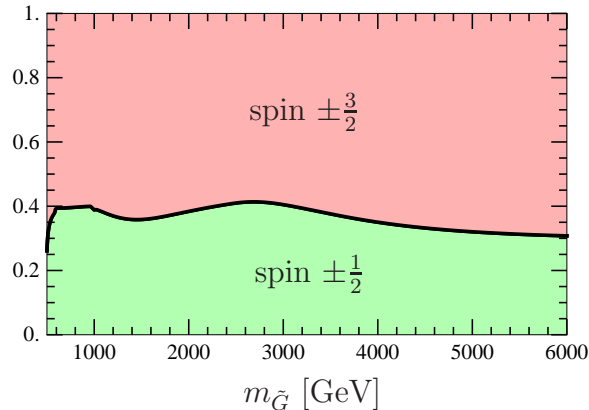


Figure 13: The relative contribution of the  $\pm\frac{1}{2}$  gravitino states (green region up to the black curve) to the total gravitino width, as a function of the gravitino mass. The remaining part (salmon color) corresponds to the relative contribution of the  $\pm\frac{3}{2}$  spin states to the total gravitino decay width. For this figure the CMSSM point parameters are used.

models as studied here, acquires its mass by absorbing the goldstino  $\pm\frac{1}{2}$  modes.

In Figure 13, we display the sum of the contributions of the  $\pm\frac{1}{2}$  gravitino spin states (green region), relatively to the sum of the  $\pm\frac{3}{2}$  contributions (salmon region) for the CMSSM point. Again the NUHM case is very similar and thus it is not shown. We see that for  $m_{\tilde{G}}$  up to about 3 TeV the  $\pm\frac{1}{2}$  states contribute up to 40% to the total decay width. The remaining 60% is due to the  $\pm\frac{3}{2}$  spin states. Eventually, for larger gravitino masses the  $\pm\frac{1}{2}$  spin states contribute about 30% of total width, this contribution remaining constant for much larger values of the gravitino mass. The reason for this is that in the gravitino decay amplitudes the center of mass energy  $\sqrt{s}$  of the process is actually the gravitino mass  $m_{\tilde{G}}$ . Hence, we are far from the high-energy limit ( $\sqrt{s} \gg m_{\tilde{G}}$ ), in which one expects the goldstino ( $\pm\frac{1}{2}$ ) components to be dominant.

## 4 Conclusions

We have presented results from a new calculation of the gravitino decay width in the context of supersymmetric models, where  $R$ -parity is conserved. This calculation includes all two-body decay channels  $\tilde{G} \rightarrow \tilde{X} Y$  where  $\tilde{X}$  is a sparticle decaying as  $\tilde{X} \rightarrow \tilde{\chi}_1^0 X$ .  $X$  and  $Y$  are SM particles, and  $\tilde{\chi}_1^0$  is the lightest neutralino that plays the role of the LSP. In addition, we have also calculated the contributions of the three-body decay channels  $\tilde{G} \rightarrow \tilde{\chi}_i^0 X Y$ . Especially the computation of the three-body decays is quite a complicated task. For this purpose we have used the packages `FeynArts` and `FormCalc` that perform symbolic

analytic calculations. In those packages we have added appropriate modules in order to accommodate them for particles with spin  $3/2$  like the gravitino. Furthermore, we have used the Weyl-van-der-Waerden formalism which considerably simplifies the treatment of the complex spin structure of the three-body gravitino decay amplitudes and enables us to calculate the individual contributions of each gravitino spin state to the total decay width.

An important advantage of our calculation of the gravitino three-body decay amplitudes, is that it treats automatically the intermediate exchanged particles that are on their mass shell by using the narrow width approximation. In such a way, we not only avoid the double counting among the two- and three-body channels, but we also improve the performance of the numerical phase space integration over the unstable exchanged particles in the propagators.

In our numerical analysis, we have chosen four representative points: two points based on the pMSSM model and two other based on the CMSSM and NUHM1 models. These points satisfy all the recent high energy experimental constraints from LHC and LHCb, but also the cosmological constraints from WMAP, Planck, and XENON100.

We have found that the knowledge of the complete three-body decay amplitude with a neutralino is important in order to compute precisely the gravitino width for any gravitino mass, not only below the mass thresholds of the dominant two-body decay channels, but also above them. Moreover, comparing the full gravitino decay width, up to the three-body level, with a previously used approximation we have demonstrated that the full result can be quite different, especially for  $m_{\tilde{g}}$  in the range 2–4 TeV. This difference is reflected also in the gravitino lifetime that we know is an important parameter to constraint models with unstable gravitinos adopting the BBN predictions. In addition, we have found that all the gravitino spin states ( $\pm\frac{1}{2}$  and  $\pm\frac{3}{2}$ ) contribute at the same order of magnitude, even for quite large gravitino masses.

Our results have been calculated using the code `GravitinoPack` that will be publicly released soon. This package incorporates various FORTRAN and MATHEMATICA routines that compute all the discussed two- and three-body gravitino branching ratios and the gravitino decay width. In addition, `GravitinoPack` will calculate analogous decay widths for the complementary case where the gravitino is stable and the LSP.

## Acknowledgements

This work is supported by the Fonds zur Förderung der wissenschaftlichen Forschung (FWF) of Austria, project No. I 297-N16. The authors thank Thomas Hahn for helpful discussions regarding the implementation of particles with spin  $3/2$  into FeynArts and they are grateful to Walter Majerotto for the careful reading of the manuscript. V.C.S. was supported by Marie Curie International Reintegration grant SUSYDM-PHEN, MIRG-CT-2007-203189.

## References

- [1] D. Lindley, *Astrophys. J.* **294** (1985) 1.
- [2] J. R. Ellis, D. V. Nanopoulos and S. Sarkar, *Nucl. Phys. B* **259** (1985) 175.
- [3] D. Lindley, *Phys. Lett. B* **171** (1986) 235.
- [4] R. J. Scherrer and M. S. Turner, *Astrophys. J.* **331** (1988) 19.
- [5] M. H. Reno and D. Seckel, *Phys. Rev. D* **37** (1988) 3441.
- [6] S. Dimopoulos, R. Esmailzadeh, L. J. Hall and G. D. Starkman, *Astrophys. J.* **330**, 545 (1988); S. Dimopoulos, R. Esmailzadeh, L. J. Hall and G. D. Starkman, *Nucl. Phys. B* **311** (1989) 699.
- [7] J. R. Ellis, G. B. Gelmini, J. L. Lopez, D. V. Nanopoulos and S. Sarkar, *Nucl. Phys. B* **373** (1992) 399.
- [8] M. Kawasaki and T. Moroi, *Prog. Theor. Phys.* **93** (1995) 879 [arXiv:hep-ph/9403364].
- [9] M. Kawasaki and T. Moroi, *Astrophys. J.* **452**, 506 (1995).
- [10] M. Kawasaki, K. Kohri and T. Moroi, *Phys. Rev. D* **63** (2001) 103502 [arXiv:hep-ph/0012279].
- [11] K. Kohri, *Phys. Rev. D* **64** (2001) 043515 [arXiv:astro-ph/0103411].
- [12] R. H. Cyburt, J. R. Ellis, B. D. Fields and K. A. Olive, *Phys. Rev. D* **67** (2003) 103521 [arXiv:astro-ph/0211258].
- [13] K. Jedamzik, *Phys. Rev. D* **70** (2004) 063524 [arXiv:astro-ph/0402344]; K. Jedamzik, *Phys. Rev. D* **70** (2004) 083510 [arXiv:astro-ph/0405583].
- [14] M. Kawasaki, K. Kohri and T. Moroi, *Phys. Lett. B* **625** (2005) 7 [arXiv:astro-ph/0402490]; *Phys. Rev. D* **71** (2005) 083502 [arXiv:astro-ph/0408426].
- [15] R. H. Cyburt, J. Ellis, B. D. Fields, F. Luo, K. A. Olive and V. C. Spanos, *JCAP* **0910** (2009) 021 [arXiv:0907.5003 [astro-ph.CO]]; R. H. Cyburt, J. Ellis, B. D. Fields, F. Luo, K. A. Olive and V. C. Spanos, arXiv:1303.0574 [astro-ph.CO].

- [16] N. E. Mavromatos and V. C. Spanos, Phys. Rev. D **87** (2013) 035025 [arXiv:1212.6386 [hep-ph]].
- [17] R. H. Cyburt, B. D. Fields and K. A. Olive, New Astron. **6** (2001) 215 [arXiv:astro-ph/0102179].
- [18] R. H. Cyburt, B. D. Fields and K. A. Olive, Astropart. Phys. **17** (2002) 87 [arXiv:astro-ph/0105397].
- [19] F. Luo, K. A. Olive and M. Peloso, JHEP **1010** (2010) 024 [arXiv:1006.5570 [hep-ph]].
- [20] T. Hahn, Comput. Phys. Commun. **140** (2001) 418 [arXiv:hep-ph/0012260].
- [21] T. Hahn and C. Schappacher, Comput. Phys. Commun. **143** (2002) 54 [arXiv:hep-ph/0105349].
- [22] T. Hahn and M. Perez-Victoria, Comput. Phys. Commun. **118** (1999) 153 [hep-ph/9807565].
- [23] H. Weyl, The Theory of Groups and Quantum Mechanics (Dover, New York, 1931); B.L. van der Waerden, Group Theory and Quantum Mechanics (Springer-Verlag, Berlin, 1974)
- [24] S. Dittmaier, Phys. Rev. D **59** (1998) 016007 [hep-ph/9805445].
- [25] H. Eberl and V.C. Spanos, “GravitinoPack: a tool that calculates gravitino processes”, in preparation.
- [26] P. Skands et al., JHEP **407** (2004) 036 [arXiv:hep-ph/0311123].
- [27] B. C. Allanach et al., Comp. Phys. Commun. **180** (2009), 8 [arXiv:0801.0045 [hep-ph]].
- [28] J. Pradler, “Electroweak Contributions to Thermal Gravitino Production”, Diploma Thesis, arXiv:0708.2786 [hep-ph].
- [29] W. Rarita and J. Schwinger, Phys. Rev. **60** (1941) 61.
- [30] P. R. Auvil and J. J. Brehm, Phys. Rev. **145** (1966) 1152.
- [31] A. Djouadi *et al.* [MSSM Working Group Collaboration], hep-ph/9901246.

- [32] M. Drees and M. M. Nojiri, Phys. Rev. D **47** (1993) 376 [hep-ph/9207234]; G. L. Kane, C. F. Kolda, L. Roszkowski and J. D. Wells, Phys. Rev. D **49** (1994) 6173 [hep-ph/9312272]; H. Baer and M. Brhlik, Phys. Rev. D **53** (1996) 597 [hep-ph/9508321]; J. R. Ellis, T. Falk, K. A. Olive and M. Schmitt, Phys. Lett. B **388** (1996) 97 [hep-ph/9607292]; A. B. Lahanas, D. V. Nanopoulos and V. C. Spanos, Phys. Rev. D **62** (2000) 023515 [hep-ph/9909497].
- [33] H. Baer, M. Brhlik, M. A. Diaz, J. Ferrandis, P. Mercadante, P. Quintana and X. Tata, Phys. Rev. D **63** (2000) 015007 [hep-ph/0005027]; J. R. Ellis, T. Falk, G. Ganis, K. A. Olive and M. Srednicki, Phys. Lett. B **510** (2001) 236 [hep-ph/0102098]; L. Roszkowski, R. Ruiz de Austri and T. Nihei, JHEP **0108** (2001) 024 [hep-ph/0106334]; U. Chattopadhyay, A. Corsetti and P. Nath, Phys. Rev. D **66** (2002) 035003 [hep-ph/0201001]; J. R. Ellis, K. A. Olive and Y. Santoso, New J. Phys. **4** (2002) 32 [hep-ph/0202110]; J. R. Ellis, K. A. Olive, Y. Santoso and V. C. Spanos, Phys. Lett. B **565** (2003) 176 [hep-ph/0303043]; M. Argyrou, A. B. Lahanas and V. C. Spanos, JHEP **0805** (2008) 026 [arXiv:0804.2613 [hep-ph]].
- [34] P. Nath and R. L. Arnowitt, Phys. Rev. D **56** (1997) 2820 [hep-ph/9701301]; H. Baer, A. Mustafayev, S. Profumo, A. Belyaev and X. Tata, Phys. Rev. D **71** (2005) 095008 [hep-ph/0412059]; H. Baer, A. Mustafayev, S. Profumo, A. Belyaev and X. Tata, JHEP **0507** (2005) 065 [hep-ph/0504001]; J. R. Ellis, K. A. Olive and P. Sandick, Phys. Rev. D **78** (2008) 075012 [arXiv:0805.2343 [hep-ph]].
- [35] G. Aad *et al.* [ATLAS Collaboration], arXiv:1208.0949 [hep-ex]; S. Chatrchyan *et al.* [CMS Collaboration], JHEP **1210**, 018 (2012) [arXiv:1207.1798 [hep-ex]]; Phys. Rev. Lett. **109**, 171803 (2012) [arXiv:1207.1898 [hep-ex]].
- [36] G. Hinshaw, D. Larson, E. Komatsu, D. N. Spergel, C. L. Bennett, J. Dunkley, M. R.olta and M. Halpern *et al.*, arXiv:1212.5226 [astro-ph.CO].
- [37] P. A. R. Ade *et al.* [Planck Collaboration], arXiv:1303.5076 [astro-ph.CO].
- [38] G. Aad *et al.* [ATLAS Collaboration], Phys. Lett. B **713**, 387 (2012) [arXiv:1204.0735 [hep-ex]]; T. Aaltonen *et al.* [CDF Collaboration], Phys. Rev. Lett. **107**, 239903 (2011) [Phys. Rev. Lett. **107**, 191801 (2011)] [arXiv:1107.2304 [hep-ex]]; updated results presented at Aspen in Feb. 2012 by M. Rescigno, <https://indico.cern.ch/getFile.py/access?contribId=28&sessionId=7&resId>

- =1&materialId=slides&confId=143360; S. Chatrchyan *et al.* [CMS Collaboration], Phys. Rev. Lett. **107**, 191802 (2011) [arXiv:1107.5834 [hep-ex]]; R. Aaij *et al.* [LHCb Collaboration], Phys. Lett. B **699** (2011) 330 [arXiv:1103.2465 [hep-ex]]; arXiv:1203.4493 [hep-ex]; For an official combination of the ATLAS, CMS and LHCb results, see: ATLAS, CMS, and LHCb Collaborations, <http://cdsweb.cern.ch/record/1452186/files/LHCb-CONF-2012-017.pdf>.
- [39] R. Aaij *et al.* [LHCb Collaboration], Phys. Rev. Lett. **110**, 021801 (2013) [arXiv:1211.2674 [hep-ex]].
- [40] G. Aad *et al.* [ATLAS Collaboration], Phys. Lett. B **716**, 1 (2012) [arXiv:1207.7214 [hep-ex]]; S. Chatrchyan *et al.* [CMS Collaboration], Phys. Lett. B **716**, 30 (2012) [arXiv:1207.7235 [hep-ex]].
- [41] E. Aprile *et al.* [XENON100 Collaboration], Phys. Rev. Lett. **107** (2011) 131302 [arXiv:1104.2549 [astro-ph.CO]].
- [42] J. Ellis, F. Luo, K. A. Olive and P. Sandick, arXiv:1212.4476 [hep-ph].
- [43] W. Porod, Comput. Phys. Commun. **153** (2003) 275 [hep-ph/0301101]; W. Porod and F. Staub, Comput. Phys. Commun. **183** (2012) 2458 [arXiv:1104.1573 [hep-ph]].
- [44] M. Frank, T. Hahn, S. Heinemeyer, W. Hollik, H. Rzehak and G. Weiglein, JHEP **0702** (2007) 047 [hep-ph/0611326]; G. Degrossi, S. Heinemeyer, W. Hollik, P. Slavich and G. Weiglein, Eur. Phys. J. C **28** (2003) 133 [hep-ph/0212020].
- [45] J. Ellis and K. A. Olive, Eur. Phys. J. C **72** (2012) 2005 [arXiv:1202.3262 [hep-ph]].